Optically-Based Diagnostics for Gas-Phase Laser Development

Wilson T. Rawlins,* Seonkyung Lee, Kristin L. Galbally-Kinney, William J. Kessler,
Adam J. Hicks, Ian M. Konen, Emily P. Plumb, and Steven J. Davis

Physical Sciences Inc.
20 New England Business Center
Andover, MA 01810-1077

ABSTRACT

In this paper we describe several diagnostics that we have developed to assist the development of high power gas phase lasers including COIL, EOIL, and DPAL. For COIL we discuss systems that provide sensitive measurements of $O_2(a)$, small signal gain, iodine dissociation, and temperature. These are key operational parameters within COIL, and these diagnostics have been used world-wide to gain a better understanding of this laser system. Recently, we have developed and integrated a similar suite of diagnostics for scaling the EOIL system and will provide examples of current studies. We are also developing diagnostics for the emerging DPAL laser. These include monitors for small signal gain that will provide both a more fundamental understanding of the kinetics of DPAL and valuable data for advanced resonator design. We will stress the application of these diagnostics to realistic laser systems.

High energy gas laser, Diagnostics, Singlet molecular oxygen, Electric discharge, Oxygen-iodine laser, Alkali laser

1. INTRODUCTION

The application of species-specific optical diagnostics has proven to be of great value in the rapid development of advanced high-energy gas-phase laser technology, including the Chemical Oxygen Iodine Laser (COIL), Electric Oxygen Iodine Laser (EOIL), Diode-Pumped Alkali Laser (DPAL), and Exciplex Alkali Laser (XPAL). The papers at this Symposium are testaments to this development. Each of these laser systems involves a unique, complex set of energetic precursor species and chemical reactions that influence the production and loss of the critical lasant species. The chemistry of these high-energy reacting mixtures is often at the edge of our understanding of molecular reaction dynamics. Thus many of the key processes are unexpected and/or unknown unless the reaction system can be interrogated with quantitative and definitive optical methods. During the history of COIL development, such interrogation was difficult and challenging owing to the limited technology for detectors, optics, and light sources, particularly in the near-infrared.[1] In recent years, dramatic improvements in solid-state detector array technology in the visible and near-infrared, as well as the advent of reliable tunable diode lasers and light-emitting diodes, have opened the doors to a new generation of optical and spectroscopic diagnostics which can probe essentially every significant reactive species in the system.[1,2] This multi-diagnostic approach imposes rigid constraints on kinetics models, which must account for all of the observed species behaviors in order to be credible for scaling predictions. The diagnostics we discuss here are highly sensitive, and can be used not only in the lasing environment but also in subscale reactors where low reagent concentrations are used to isolate the most important processes.

In our research at PSI, we have focused for several years on the kinetics and dynamics of EOIL, including electric discharge excitation in oxygen-argon and oxygen-helium mixtures, chemical reactions within the energetic active-oxygen discharge effluent, the reactions of active-oxygen species with molecular and atomic iodine, and inversion of the atomic iodine state populations to achieve gain and lasing.[3-9] During the course of this work, we have developed a multi-diagnostic suite to routinely determine the concentrations of the key species $O_2(a^1\Delta_g)$, $O(^3P)$, O_3, I_2, $I(^2P_{3/2})$, and $I(^2P_{1/2})$, as well as small-signal gain and gas temperature. Table 1 summarizes these diagnostics. Many of these systems also have direct application to advanced COIL systems research and development.[10] More recently, we have begun investigations of DPAL and XPAL dynamics, including observations of alkali-rare-gas exciplex-assisted absorption and laser-induced fluorescence, and multi-photon excitation of infrared atomic alkali transitions.[11,12] In this paper, we focus on very recent results in the development of a gain diagnostic for optically pumped alkali D-line transitions. We describe the technical approach for each of the EOIL diagnostics and the DPAL gain diagnostic, and present brief examples of representative measurement results and system implications for each.

Report Documentation Page

Form Approved
OMB No. 0704-0188

1. REPORT DATE	2. REPORT TYPE	3. DATES COVERED
AUG 2010		**00-00-2010 to 00-00-2010**

4. TITLE AND SUBTITLE	5a. CONTRACT NUMBER
Optically-Based Diagnostics for Gas-Phase Laser Development	5b. GRANT NUMBER
	5c. PROGRAM ELEMENT NUMBER
6. AUTHOR(S)	5d. PROJECT NUMBER
	5e. TASK NUMBER
	5f. WORK UNIT NUMBER
7. PERFORMING ORGANIZATION NAME(S) AND ADDRESS(ES) **Physical Sciences Inc,20 New England Business Center,Andover,MA,01810-1077**	8. PERFORMING ORGANIZATION REPORT NUMBER
9. SPONSORING/MONITORING AGENCY NAME(S) AND ADDRESS(ES)	10. SPONSOR/MONITOR'S ACRONYM(S)
	11. SPONSOR/MONITOR'S REPORT NUMBER(S)

12. DISTRIBUTION/AVAILABILITY STATEMENT
Approved for public release; distribution unlimited

13. SUPPLEMENTARY NOTES
SPIE XVIII International Symposium on Gas Flow and chemical Lasers and High Power Lasers 2010, Sofia, Bulgaria, August 30 - September 3, 2010. U.S. Government or Federal Rights License

14. ABSTRACT
In this paper we describe several diagnostics that we have developed to assist the development of high power gas phase lasers including COIL, EOIL, and DPAL. For COIL we discuss systems that provide sensitive measurements of O2(a), small signal gain, iodine dissociation, and temperature. These are key operational parameters within COIL and these diagnostics have been used world-wide to gain a better understanding of this laser system. Recently, we have developed and integrated a similar suite of diagnostics for scaling the EOIL system and will provide examples of current studies. We are also developing diagnostics for the emerging DPAL laser. These include monitors for small signal gain that will provide both a more fundamental understanding of the kinetics of DPAL and valuable data for advanced resonator design. We will stress the application of these diagnostics to realistic laser systems.

15. SUBJECT TERMS

16. SECURITY CLASSIFICATION OF:			17. LIMITATION OF ABSTRACT	18. NUMBER OF PAGES	19a. NAME OF RESPONSIBLE PERSON
a. REPORT	b. ABSTRACT	c. THIS PAGE			
unclassified	**unclassified**	**unclassified**	**Same as Report (SAR)**	**14**	

Table 1. Diagnostics Used to Characterize the Discharge Laser Devices

Species or Parameter	Method	Wavelength
I*, I, T	TDL Absorption/Gain	1315 nm
O_2(a,b), I*	InGaAs array emission spectrometer	700-1500 nm
O	NO-O chemiluminescence	580 nm
I_2 flow rate	LED micro-absorption	488 nm
Ozone	UV micro-absorption	254 nm
I_2 (B)	Visible emission spectrometer	500-700 nm

2. EOIL DISCHARGE-FLOW REACTORS

First, a general and brief introduction to the operating principles of EOIL is in order; subsequent papers in this Symposium will fill in the details. EOIL is an oxygen-iodine laser where the metastable singlet oxygen is generated by an electric discharge. The discharge also generates atomic oxygen, which reacts rapidly with I_2 vapor to produce atomic iodine. The lasing state, $I(^2P_{1/2})$ or I*, is excited by the reversible energy transfer reaction:

$$O_2(a) + I \rightleftarrows O_2(X) + I^*$$

The equilibrium of this reaction shifts to the right at lower temperatures, hence a supersonic expansion is used to achieve high gain. The electric discharge methods employed (high power microwave, radio frequency, and pulser-sustainer) typically operate on mixtures of O_2 and helium and produce several energetic species. Most of these species are short-lived after the gas exits the active discharge. O atoms and O_2(a) are the primary energetic species that survive into the reaction zone, where I_2 is introduced into the flow stream. A typical system is illustrated in Figure 1.

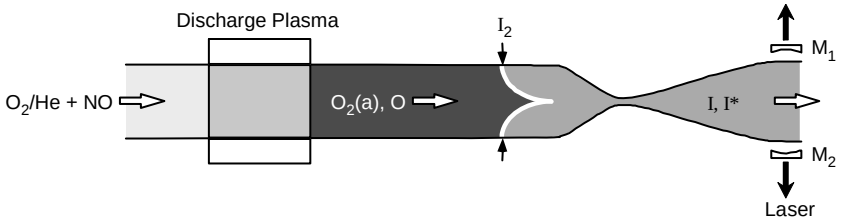

Figure 1. Diagram of an open-cycle EOIL. Several regions of the flow are indicated. M_1 and M_2 denote the mirrors for a stable optical resonator.

The conventionally accepted mechanism for the reactions between I_2 and the effluent of the oxygen discharge is[4,5]

$$\begin{aligned}
O + I_2 &\rightarrow IO + I && I_2 \text{ dissociation} \\
O + IO &\rightarrow O_2 + I && \\
O_2(a) + I &\rightleftarrows O_2(X) + I^* && I^* \text{ excitation (near-resonant, reversible)} \\
O + I^* &\rightarrow O + I && I^* \text{ quenching} \\
I^* &\rightarrow I + h\nu && \text{Lasing}
\end{aligned} \qquad (1)$$

Atomic oxygen provides rapid dissociation of I_2, so that no O_2(a) is lost in the dissociation step. However, atomic oxygen in large concentrations also quenches I*, so its concentration must be actively controlled. This is done by addition of NO_2 or NO, using the coupled reactions

$$\begin{aligned}
O + NO + M &\rightarrow NO_2 + M \\
O + NO_2 &\rightarrow NO + O_2
\end{aligned} \qquad (2)$$

to reduce the O concentration (where M signifies a generic third-body collision partner, e.g. O_2 and He). A large body of work has demonstrated that when sufficient NOx is introduced to the reacting flow, the optical gain is greatly increased and is sufficient to support lasing.[3,4,9,13,14] Recent work by Carroll and coworkers has demonstrated the scaling of gain, power in the flow, and laser power to high levels, with outcoupled laser power exceeding 100 W.[15] Other recent work at PSI is pursuing a hybrid EOIL concept in which an iodine oxide catalyst is used to enhance the singlet oxygen yields above the levels produced by the discharge.[16-19]

At PSI, we use microwave discharge techniques to generate the active oxygen species in two different discharge-flow reactors, both of which have a high degree of optical access for diagnostic measurements. One of these is a conventional, low-pressure, subsonic flow reactor illustrated in Figure 2. The main gas flow, a mixture of O_2 and He, passes through a resonant-cavity microwave discharge (2.45 GHz, 50-100 W, 10-100 Td) and into the main flow reactor (~5 cm i.d.), where the reagents are added through fixed-place or movable inlets. The species detection is carried out at purged window ports downstream of the reaction zone. Typical flow conditions are 1-5 mmole/s, 1-10 Torr, 300-350 K, with flow velocities in the range of 500-2000 cm/s. This apparatus is ideal for investigations of active oxygen kinetics, and for diagnostic concept development.

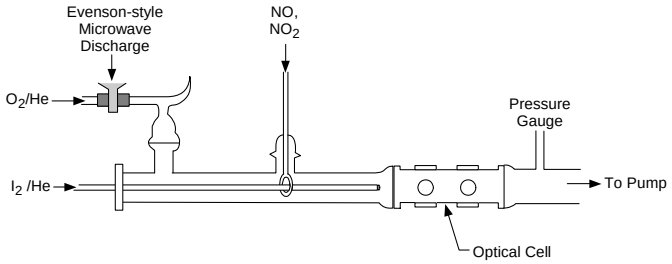

Figure 2. Low-pressure microwave discharge-flow reactor

In order to exercise the diagnostics and test the kinetics concepts in practical EOIL conditions, we have also developed the supersonic laser-reactor illustrated in Figure 3.[7,8] This apparatus uses a coaxial 2.45 GHz microwave discharge, based on PSI's MIDJet technology, at powers of 1 to 5 kW, E/N 10 to 50 Td, pressures of 30 to 70 Torr, and flow rates of 40 to 100 mmole/s. The chemically reacting flow is expanded to Mach ~2 through an optically accessible cavity. Optical measurements are made through purged windows in both the subsonic and supersonic flow sections. Power extraction, by max-R mirrors in a stable resonator configuration, is typically 100 to 150 mW, with a measured beam quality $M^2 = 1.08 \pm 0.01$.[8]

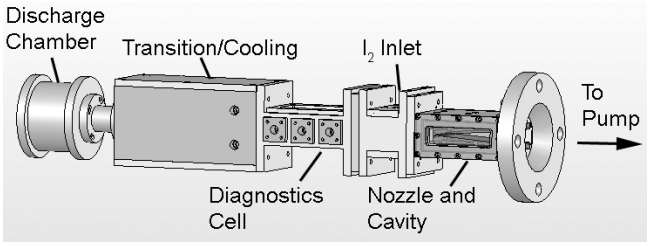

Figure 3. EOIL subsonic/supersonic flow reactor

3. NEAR-INFRARED ABSOLUTE EMISSION: $O_2(a)$ AND I*

We determine the $O_2(a)$ and I* concentrations by observing their emission spectra in the $O_2(a^1\Delta_g \rightarrow X^3\Sigma_g^-)$ and $I(^2P_{1/2} \rightarrow {}^2P_{3/2})$ transitions, at 1270 and 1315 nm respectively. The concentrations are determined from the fundamental relationship[20] that the band-integrated emission intensity of each transition, in photons/cm^3-s, is equal to the product of the $O_2(a)$ or I* concentration and the band-averaged Einstein coefficient for the transition. We observe the emission spectrum with a calibrated spectrometer, integrate over the band, and divide by the Einstein coefficient to determine absolute values of $[O_2(a)]$ and [I*]. The $O_2(a \rightarrow X)$ and $I^* \rightarrow I$ emission spectra are observed by a Roper Scientific liquid-nitrogen-cooled, 512-element InGaAs array detector. The array is mounted in the exit plane of a monochromator equipped with a 600 line/mm grating blazed at 1000 nm wavelength. This grating disperses the emission spectrum across a portion of the array. The spectral resolution is controlled by micrometer adjustment of the entrance slit width of the monochromator, and is typically set to ~0.3 nm. The emission from the field of view is collected and transmitted to the entrance slit by a 3-m long optical fiber bundle. The fiber bundle mates to the entrance slit via a rectangular adapter matching the vertical dimension of the slit, such that all of the light transmitted by the bundle passes through the entrance slit. The light-collecting end of the bundle, which is mounted on the optical cell, is custom-adapted to include a collimating lens and aperture. The lens is an f/0.75 plano-convex aspheric lens (Melles-Griot 01 LAG 005), and converts the fiber bundle's highly divergent acceptance cone into a near-collimated field of

view along a 15 cm length. The combination of the lens and aperture confine the diameter of the field of view to 13 mm at the near window and 15 mm at the far window. Thus the only reactor surfaces within the field of view are non-reflective windows, so there is no possibility of observing contributions of internally reflected emission from upstream or downstream of the measurement volume. This is an exceptionally important consideration in discharge-driven systems, where stray light from the active discharge (e.g. atomic Rydberg transitions) can enter the field of view and give misleading results if one is not careful.

Figure 4 illustrates the field of view collimation and calibration methods. The absolute spectral responsivity of the instrument is determined through photometric calibrations using a NIST-traceable, 1000 C blackbody radiation source. The blackbody radiation source is placed at a distance from the collecting optic which is identical to the distance to the center of the field of view in the experimental measurements. The diameter of the blackbody aperture is set to 22 mm, to provide an extended source larger than the field of view diameter as in the experiments. Measurements with several aperture diameters verify that this condition is satisfied, i.e. that the observed radiance is independent of the blackbody aperture diameter above ~16 mm.

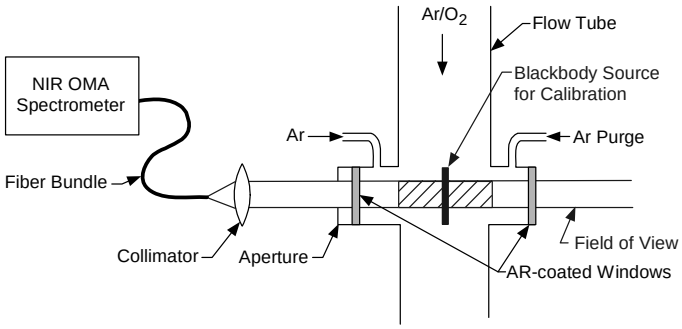

Figure 4. Illustration of the field of view and calibration method for the NIR emission spectrometer.

For both the blackbody and the experimental gas emission measurements, the observed signal (e.g., counts/s) is proportional to the absolute intensity I(λ) (e.g., photons/cm^2-s-sr-nm) through the product of the spectral responsivity function F(λ), an optical transmission T(λ) for the overall system, a spectral bandpass δλ, and the etendue or AΩ product, where A and Ω are the area and solid angle of the field of view, respectively:

$$S(\lambda) = F(\lambda)\, T(\lambda)\, A\Omega\, \delta\lambda\, I(\lambda)$$

Since the field of view in both cases is collimated and limited by the collection aperture, it is straightforward to show that AΩ is the same for both the calibration and the gas emission measurement geometries. In addition, the calibrations use the same optical transmission and spectral bandpass as the gas emission measurements. If we take the ratio of the blackbody and gas signals, the geometry-specific factors cancel, and the absolute intensity of the gas emission is simply

$$I_{gas}(\lambda) = S_{gas}(\lambda) / F(\lambda)$$

where the responsivity F(λ) is determined from the blackbody data:

$$F(\lambda) = S_{BB}(\lambda) / N(\lambda, T_{BB})$$

$N(\lambda,T_{BB})$ is the Planck radiation formula for the spectral radiant intensity from a Lambertian blackbody at temperature T_{BB} and unit emissivity. This approach results in highly accurate determinations of the spectral responsivity and gas emission intensity that are affected only by uncertainties in the temperature of the blackbody source. Our measurements of F(λ) for blackbody temperatures from 800 to 1000 C indicate radiance errors of <1%.

In practice, the spectral responsivity function determined in the calibration is applied to the baseline-corrected $O_2(a)$ and I* emission spectra to convert the intensities into absolute units, e.g. photons/cm^3-s-nm. Integration of each spectrum over the spectral band and division by the Einstein coefficient for the transition then gives the $O_2(a)$ and I* concentrations, $[O_2(a)]$ and [I*], in molecules/cm^3. Historically, the Einstein coefficient for the $O_2(a \rightarrow X)$ transition

has been poorly known despite numerous measurements and theoretical calculations. More recently, a series of high-resolution absorption measurements by three different techniques gives excellent agreement on the value $A_{a\text{-}X}$ = 2.2 x 10^{-4} s^{-1}, with a 2σ error estimate of ~ 10%.[21,22] The systematic uncertainty in this value is the dominant uncertainty in the [O_2(a)] determination. For 0.3 nm spectral resolution, our instrument has an O_2(a) detection limit of ~5 x 10^{12} cm^{-3} for the maximum practical integration time of 90 seconds and a path length of 5 cm across the flow. This provides excellent signal-to-noise ratio and dynamic range for typical discharge-flow concentrations of 10^{14}-10^{15} cm^{-3}. Similarly, the Einstein coefficient for I*→I is 8.0 s^{-1} with an estimated uncertainty of ±20%.[23] Our detection limit in this case is ~10^8 cm^{-3}, far below the typical observed values of 10^{12}-10^{13} cm^{-3}. The extraordinary sensitivity of the InGaAs array spectrometer allows us to pursue fundamental kinetics measurements at low reagent concentrations in the subscale reactor, eliminating interferences from side reactions.

We further analyze the O_2(a→X) emission spectra by a least-squares spectral fitting procedure to determine rotational temperatures and vibrational population distributions. Spectral emission lines computed from spectroscopic first principles are convolved with the instrument spectral scanning function, and are compared to each observed spectrum to determine the best least squares fit. The solutions are the rotational temperature and vibrational state populations in the O_2(a) state. Example observed and computed best-fit spectra from the subsonic and supersonic sections of the MIDJet/EOIL reactor are shown in Figure 5. The observed subsonic and supersonic temperatures are in excellent agreement with translational temperatures determined from atomic iodine linewidths by tunable diode laser absorption spectroscopy when I_2 is injected into similar flows. They also agree well with flow temperatures computed from FLUENT CFD calculations.[7,8]

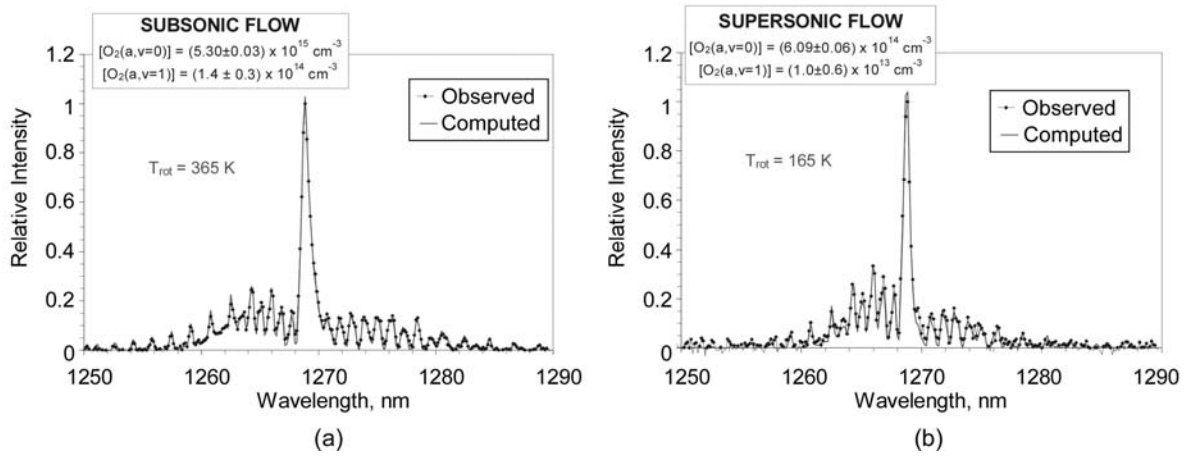

Figure 5. Observed and best-fit computed spectra of O_2(a→X) emission in MIDJet/EOIL reactor: (a) subsonic flow prior to nozzle; (b) supersonic flow. Least squares fit concentrations and rotational temperatures are indicated on the plots.

We have used the spectral fitting method to examine the contributions to the emission from vibrationally excited O_2(a,v) via the (1,1), (2,2), and (3,3) bands. These bands are shifted to slightly longer wavelengths corresponding to the vibrational anharmonicity of the a-state. We have estimated the Einstein coefficients for these transitions by scaling from the (0,0) value according to the Franck-Condon factors[24] $q_{v'v"}$ and transition moment R as a function of r-centroid r:[20]

$$A_{v'v"} = (64\pi^4/3h)\,(\nu^3 q_{v'v"})\,(R(r))^2$$

We have estimated the scaling of $(R(r))^2$ by fitting this equation to the relative values A_{00}:A_{01}:A_{10}, using our measurements[25] of A_{00}/A_{01} = 52 ± 6 and atmospheric observations[26] of a lower bound A_{00}/A_{10} > 200. The results give A_{11} = 2.17 x 10^{-4} s^{-1}, A_{22} = 2.12 x 10^{-4} s^{-1}, and A_{33} = 2.06 x 10^{-4} s^{-1}, i.e. very little variation with v'.

The spectral analysis confirms that essentially all of the observed emission is due to the (0,0) band of the a→X system, i.e. there is little or no observable vibrational excitation of the O_2(a). The Q-branch of the (1,1) transition, which should appear at 1280.5 nm if O_2(a,v=1) is populated, is near or below our detection limit in all cases. The O_2(a,v=1) populations determined by least squares spectral fitting are typically 3% to 7% of the total O_2(a)

concentration, and is based entirely on the fitting of the (1,1) Q-branch structure to a single feature at 1280.5 nm as shown in Figure 6.

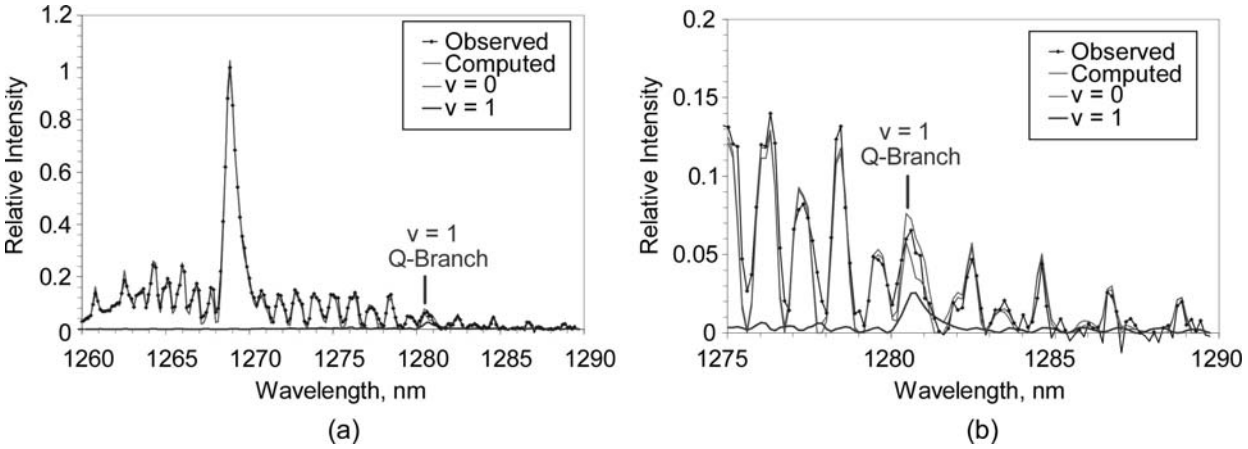

Figure 6. Spectral fit of $O_2(a \rightarrow X)$ emission illustrating the v=0 and v=1 contributions.

The notable absence of vibrationally excited levels in the spectrum is a consistent result over a wide range of conditions, near the discharge exit and far downstream, for 50 W to 2 kW discharge powers, 0.5 to 50 Torr, high and low flow velocities, and even in COIL conditions using Cl_2/BHP generation of $O_2(a)$ at large concentrations and energy pooling conditions. This suggests very rapid energy exchange between $O_2(a,v)$ and $O_2(X,v=0)$. This is reasonable in view of the closely matched vibrational frequencies of the two states, and is consistent with experimental measurements described by Slanger and Copeland.[27] This finding is very important to considerations of the role of $O_2(a,v)$ in the COIL I_2 dissociation mechanism.

4. DETERMINATION OF [O] BY AIR AFTERGLOW EMISSION: O + NO

The atomic oxygen concentrations are determined by the air afterglow method, where known flow rates of NO are injected into the discharge effluent flow and [O] is determined from the intensity of the O + NO chemiluminescence observed with a bandpass-filtered photomultiplier tube at 580 nm. The air afterglow is spectrally continuous emission from 390 nm to >3 μm, arising from rovibronically excited NO_2^* produced in the very slow, pressure-independent recombination of O and NO. We have assembled a well-collimated, fiber-coupled photometer with a photomultiplier and a 10-nm bandpass filter centered at 580 nm. The field of view of the collection fiber is collimated to ~6 mm diameter across the flow field and is directed toward an opposing window, so that no reflective wall surfaces are observed. We have calibrated the photometer in two ways, using both the well-known N + NO titration method and a radiometric blackbody calibration. The overall accuracy of the [O] determinations is ±5%.

To determine [O] in the low-pressure flow reactor, we observe the 580 nm photometer signal for a series of NO flow rates, giving straight-line fits as illustrated in Figure 7. The slopes of these lines are proportional to the O concentration through a constant including the field-of-view calibration factor and the conversion of NO flow rate to concentration. These particular experiments were designed to probe the dependence of O-atom production on the gas residence time in the active discharge, by varying the total flow velocity at a constant pressure and O_2/He mixing ratio. The resulting [O] determinations are shown in Figure 8, compared to $O_2(a)$ determinations by the NIR emission method. These results relate to models of the discharge production kinetics which we will not discuss here. However, the figure illustrates a key point: through systematic, calibrated diagnostics of specific species concentrations, we can test our preconceived ideas of how complex chemical systems work. In this case, we consistently observe discharge production ratios $[O]/[O_2(a)] \leq 1$; this is in marked contrast to discharge model predictions, which give $[O]/[O_2(a)] >> 1$ for these discharge conditions. This magnitude of discrepancy between observation and expectation suggests a large uncertainty in the electron-impact dissociation cross sections for O_2, and is highly relevant to modeling and scaling applications for EOIL.

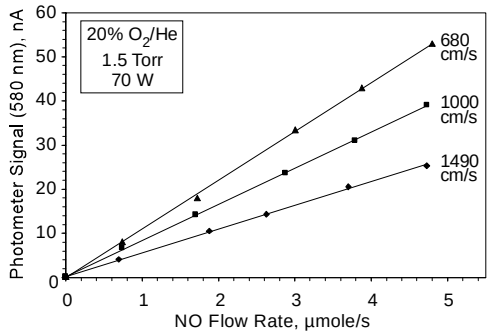

Figure 7. Example plots of 580 nm photometer signal vs. NO flow rate for the flow conditions given in the legend.

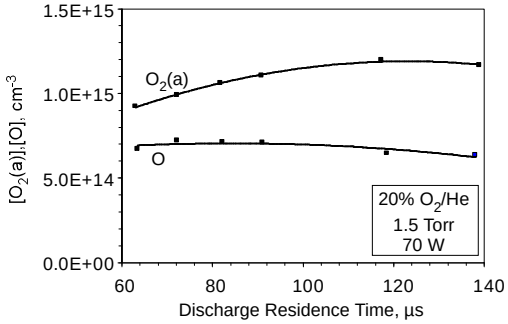

Figure 8. Example plots of [O] and [O_2(a)] measurements as functions of gas residence time in the discharge.

We have used the air afterglow technique to estimate O-atom yields in the subsonic flow MIDJet/EOIL reactor. In this case, the three-body O loss effect due to NOx reactions is quite large, so an alternative approach is to analyze the decrease in intensity, due to O removal, as a function of increasing [NO]. The result is an exponential decay, which can be extrapolated to zero NO to determine [O] at the measurement station. As in the case of the low-pressure system, we observe much lower O-atom yields than we predict from discharge models of the electron-impact processes. The method also provides a convenient way to image the flow field in both the subsonic and supersonic flow sections.

5. ULTRASENSITIVE ABSORPTION: O_3 AND I_2

O_3 and I_2 can be detected by direct absorption, at 253.7 and 488 nm respectively. However, due to the low concentrations and short path lengths in typical EOIL and COIL reactors, the absorbances are usually very small and difficult to detect with conventional 12- or 14-bit data acquisition systems. We have developed a dual-beam ratiometric method with a high-precision, low-noise electrometer-amplifier system that gives ~20-bit sensitivity. Molecular absorbances can be measured down to levels of ~10^{-5} or less, approaching the shot noise limit. Figure 9 illustrates the optical setups for the O_3 and I_2 absorption diagnostics; each diagnostic is operated independently. The I_2 diagnostic uses a blue LED light source with a 488 nm narrow-band filter on each detector; the light beam is shaped and collimated by a telescope and a lens prior to entering the reactor. A corner reflector is used to give a folded path configuration. A beamsplitter reflects some of the light onto a reference detector; the remainder of the light passes through the reactor and the transmitted portion passes to the detector photodiode. An adjustable aperture on the entrance to the beamsplitter housing controls the intensity and size of the probe beam. The O_3 monitor has a similar arrangement, with a mercury pen lamp light source and no lenses.

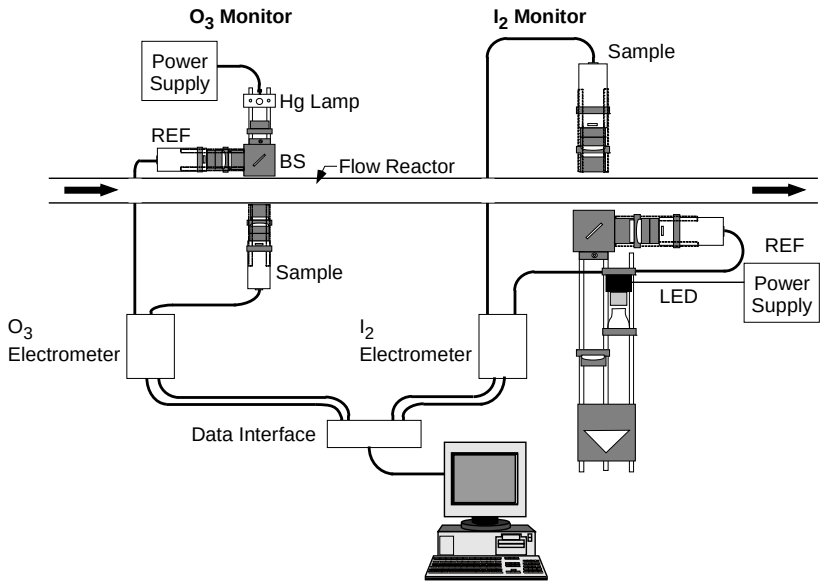

Figure 9. Schematic of optical setup or O_3 and I_2 diagnostics on a generic flow system.

We have used the I_2 diagnostic to confirm the measured I_2 flow rates in the reactors, and to determine the degree of I_2 dissociation in both EOIL and COIL systems. We have used the O_3 diagnostic to quantify O_3 concentrations in the MIDJet/EOIL system, and to investigate the role of O_3 in the kinetics of discharge-generated active oxygen. For example, through comparative measurements of [O_3] and [O] in the discharge effluent at several pressures and reaction times, we have discovered that the two species are in near-steady state, rather than the expected exponential loss of O and build-up of O_3 due to three-body recombination of O with O_2.[6] This observation is evidence for the reaction of O_2(a) to dissociate O_3(v) as it is formed in the recombination process:[28]

$$O + O_2 + M \rightarrow O_3(v) + M$$
$$O_2(a) + O_3(v) \rightarrow O_2 + O_2 + O$$

This result has a significant bearing on model predictions of the evolution of O and O_3 in the plenum flows of EOIL reactors.

6. SMALL-SIGNAL GAIN: ATOMIC IODINE

We monitor the small-signal gain on the atomic iodine transition with a scanning tunable diode laser on the (F'=3,F"=4) hyperfine line of I($^2P_{3/2}$—$^2P_{1/2}$) at 1315 nm. This sensor has been described in detail elsewhere[3-5] and is now widely used in development of COIL and EOIL systems around the world. The measurement approach uses balanced ratiometric detection of the signal (transmitted) and reference beams to achieve a detection limit for gain of ~10^{-5} %/cm. An example gain measurement in the supersonic flow of the MIDJet/EOIL reactor is illustrated in Figure 10. At typical supersonic flow pressures (1-2 Torr), the line is primarily Doppler broadened, and the gas temperature can be determined from the line width. The peak gain (or absorption) can be divided by the stimulated emission cross section to determine the quantity {[I*]-[I]/2}. When combined with the near-IR emission determination of [I*] for the same conditions, one can determine [I] and then other interesting quantities: [I*]/[I], the inversion ratio which should be directly related to the O_2(a) yield, and ([I*]+[I])/2, which should correspond to the amount of I_2 dissociated.

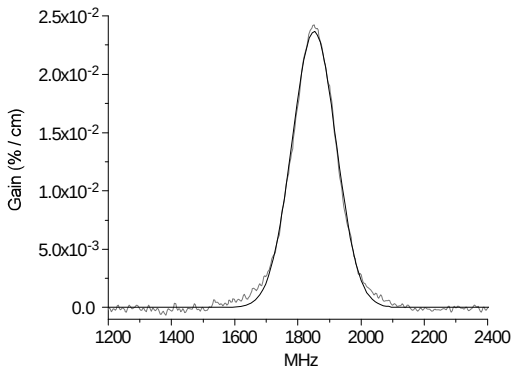

Figure 10. MIDJet/EOIL gain measurement: 4.35 cm downstream of 1.5 mm nozzle throat, 87 mmole/s total flow rate, discharge gas 5% O_2/He + 0.46 mmole/s NO, 29 μmole/s I_2, 1 kW discharge power, 72 Torr discharge pressure, 46 Torr subsonic flow pressure.

Concerted measurements of gain, I* emission, and $O_2(a)$ have been extremely valuable in addressing I* loss phenomenology in both the subscale and MIDJet/EOIL reactors. For example, in the low-pressure reactor, we have demonstrated [I*]/[I] inversion ratios well below the model-predicted near-equilibrium values, which we have ascribed to the previously unknown loss reaction[4,5]

$$I^* + O_2 \rightarrow I + O_2(v)$$

We have also observed this ratio to be substantially increased by the effect of an iodine oxide catalyst on the reactor walls.[17] In the MIDJet/EOIL system, we observe the [I*]/[I] ratio to increase with added NO concentration beyond the point of optimum gain, indicating a level of complexity in the reaction mechanism which is not accounted for in the conventional kinetics modeling scheme.[7-9] We are continuing to pursue these types of coordinated, multi-species measurements to determine a reaction mechanism which adequately accounts for the I* production and loss processes in the EOIL and catalytic-EOIL chemical systems.

7. SMALL-SIGNAL GAIN: ALKALI AND ALKALI-EXCIPLEX LASER SYSTEMS

Proper review and discussion of the DPAL and XPAL laser systems can be found elsewhere,[11,12] and in the paper by Carroll and coworkers at this Symposium.[29] We focus here on emerging results from our laboratory using the dual-beam tunable diode laser method, described above for I-atoms, to measure gain on the alkali atom transitions. The basic operation of the DPAL and XPAL laser systems is illustrated for Cs in Figure 11. Both laser concepts offer the means to couple high-power diode lasers into gas-phase absorption and laser output. In the DPAL case, shown on the right-hand edge of the figure, a pump laser (e.g. a high-power diode laser) excites the Cs D_2 transition at 852 nm, Cs($^2S_{1/2} \rightarrow {}^2P_{3/2}$), and a collision partner such as C_2H_6 deactivates the $^2P_{3/2}$ state to the $^2P_{1/2}$ state. This produces an inversion on the D_1 transition at 894 nm. DPAL requires elevated temperatures, to produce sufficient alkali atom concentrations, and elevated pressures, e.g. several hundred Torr of He, to broaden the absorption and improve spectral overlap with the spectrally broad diode laser output. (Narrow-band diode lasers are also in development.) The XPAL system takes advantage of weak van der Waals attractions between the alkali atom and larger, polarizable rare gas atoms (Ar, Kr) to broaden the absorption out to several nm, providing a good spectral match to presently available diode lasers. The absorption occurs on the X→B molecular transition, and the B-state promptly dissociates directly into the $^2P_{3/2}$ state, producing inversion on the D_1 transition. Inversion can also be created on the D_2 transition by using C_2H_6 to promote the spin-orbit transfer, as in DPAL. XPAL requires elevated temperature to increase the alkali atom concentration, and elevated rare gas pressure to promote the exciplex formation.

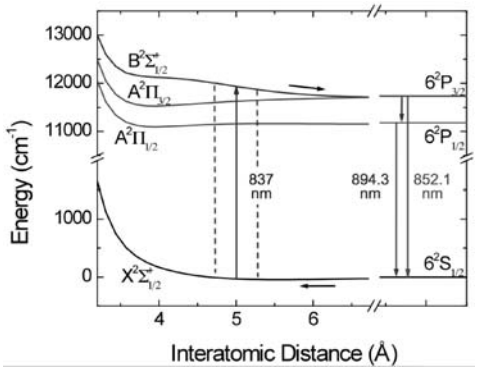

Figure 11. Potential energy diagram for Cs-Ar exciplex, illustrating operating principles of DPAL and XPAL.

Our gain measurements to date have focused on the DPAL system, pumping D_1 and probing D_2, but use XPAL configurations, e.g. Cs-Kr-C_2H_6, in sealed quartz or Pyrex cells with windows on the ends.[11,12] The cells used to date are 5 cm long, 2.5 cm diameter, and contain Cs or Rb buffered with 500 Torr of rare gas (Ar, Kr, Xe); some also contain 75 Torr of C_2H_6. The cell is encased in a small oven with apertures for laser and optical viewing access. The excitation source is a Ti:S laser which provides tunable, CW output from 750 nm to nearly 900 nm. The probe laser is a distributed-feedback, tunable diode laser in a dual-beam configuration. The TDL laser beam is split into reference and probe beams, and the probe beam is co-aligned along the axis of the Ti:S pump beam, such that the diameter of the probe beam is much less than that of the pump beam. In measurements to date, the probe beam samples the D_1 transition while the pump beam is tuned near or onto the D_2 transition. The combined beams are focused into the gas cell by a lens. After passage through the cell, a series of two diffraction gratings separates the probe beam from the pump beam and directs it to the detector. The reference and transmitted probe beam intensities are ratioed to cancel noise and normalize the drift with scanning frequency. The probe laser wavelength is rapidly and repeatedly scanned through the D_1 hyperfine multiplet to produce a signal-averaged spectral scan for a given condition. Scans with the pump laser off measure atomic absorption by the ground $^2S_{1/2}$ state for a given cell temperature (alkali vapor concentration). Scans with the Ti:S pump laser tuned to the D_2 absorption line measure the modification of the ground-state concentration caused the optical excitation, and optical gain in the event of an inversion on the D_1 transition.

The spectroscopy of alkali atom absorption near room temperature and low bath-gas pressures is straightforward and well understood through some five decades of research. However, the measurements are more complex to interpret at the elevated temperatures and pressures required for DPAL and XPAL operation, due to extensive collisional broadening and overlap of the lines. Spectral predictions and analysis must account in detail for the effects of spin-orbit coupling, hyperfine splitting, collisional broadening, and collision-induced frequency shifts, using Voigt line shapes.[12] Computed absorbance spectra for Cs in the Doppler-broadened limit and the pressure-broadened condition are compared in Figure 12. The calculations illustrate the broadening into a single unresolved feature, with Lorentzian wings extending far from the line center. This greatly extends the required scan range of the probe laser, in order to encompass the full line shape and determine the baseline signal level. In addition, the absorbance becomes highly optically thick for ground state atom concentrations characteristic of DPAL and XPAL operating conditions. Thus comparisons of the computed and observed spectra are essential for interpreting the experimental results.

When a hydrocarbon such as ethane is added to the gas mixture to promote the transfer of population from $^2P_{3/2}$ to $^2P_{1/2}$, the system functions as a conventional DPAL configuration, and large optical gain is easily observed. Figure 13 shows an example for Cs in 500 Torr Kr, 75 Torr C_2H_6 at 338 K with a 5 cm path length. Due to the limited frequency range of the probe laser scan, the wings of the lines are cut off by the baseline subtraction procedure. However, this is a small correction (<10%, cf. Fig. 12b), and the plot illustrates the development of the ground-state population inversion as the excitation intensity is increased. In this case, the inversion appears to occur initially on the F"=4 transitions (cf. Fig. 12a), and then progresses to F"=3 as the pump power increases. More detailed work is in progress, including measurements of gain in Cs and Rb as a function of hyperfine state excitation and exciplex excitation, for various temperatures (alkali concentration) and rare gas conditions.

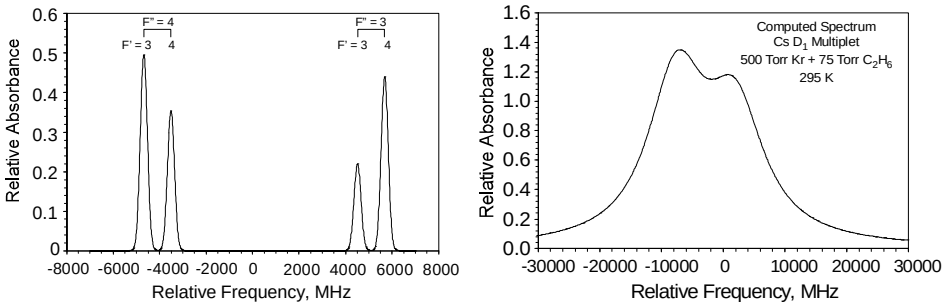

(a) (b)

Figure 12. Computed absorbance spectra for the Cs D_1 transition at 894 nm. (a) low pressure limit, Doppler broadening, illustrating the hyperfine structure; (b) high pressure, illustrating collisional broadening effects.

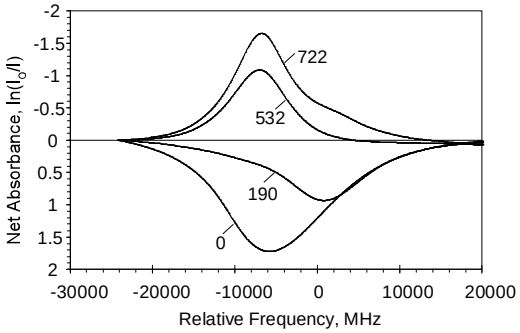

Figure 13. Absorbance and gain spectra for Cs(D_1) at 894 nm as a function of pump intensity on the D_2 line at 852 nm. Cell conditions: Cs in 500 Torr Kr and 75 Torr ethane, 338 K, 5 cm path length

This type of measurement provides a direct probe of the dynamics of the population inversion as a function of pump laser power, and aids in the design of optical resonators. Extensions of the technique can be used to examine spatial variations in the gain, e.g. for side-pumped systems. Figure 14 shows example results from a preliminary gain imaging measurement for the Cs-Kr-C_2H_6 cell of Figure 13. For this measurement, the probe beam diameter was expanded to be larger than that of the pump beam, and the transmitted probe beam was directed through neutral density filters onto the focal plane of an InGaAs camera. The figure shows images obtained with the probe laser at a fixed frequency on resonance and the pump laser off resonance (bottom image) and on resonance (top image). The color bar indicates the value of $\ln(I/I_o)$ for the 5-cm path; the light grey portion of the image signifies the region of positive gain. Peak gain at the center of the image is ~0.75 for the 5 cm gain length. Background measurements with the probe laser off resonance or blocked and the pump laser on resonance, off resonance, or blocked verified that there was no background signal from the pump laser or fluorescence from the gas. The spatial distribution of the gain follows the Gaussian distribution of the Ti:S pump laser beam. We are continuing to examine the spatial distribution as a function of pump laser intensity.

More experiments are in progress to investigate the spectrally and spatially distributed gain and absorption for a variety of cells in DPAL and XPAL configurations. We are also proceeding to gain measurements for short-path XPAL cell configurations at higher temperatures, for both Cs and Rb excitation. In related research, we are investigating exciplex-assisted multiphoton excitation effects using quantitative infrared emission spectroscopy, as described elsewhere.[11,12]

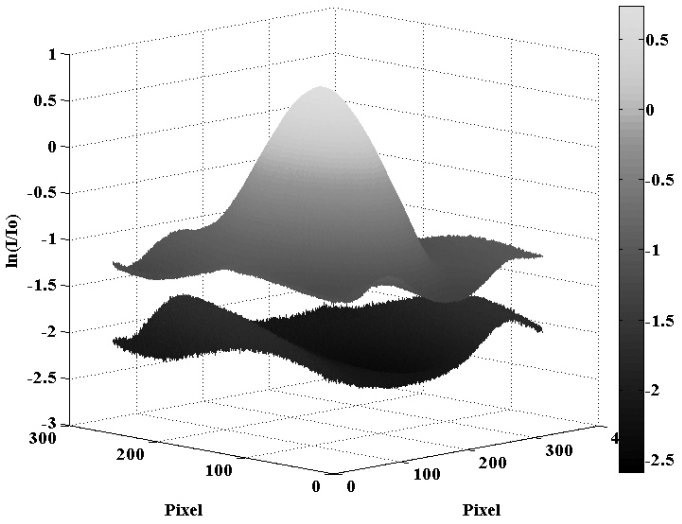

Figure 14. Three-dimensional image of spatially resolved gain and absorption on the D_1 line at a fixed probe laser frequency tuned to resonance. Upper image: pump laser on resonance with D_2 absorption resulting in gain near the center of the pump beam; lower image: pump laser off resonance, no D_2 absorption. The color bar indicates the range of gain and absorbance; light grey indicates gain.

8. CONCLUSIONS

We have described a multi-species diagnostic method which incorporates the attributes of absolute emission spectrometry, ultra-sensitive absorption photometry, and diode laser absorption/gain spectroscopy for comprehensive determinations of the key parametrics of gas laser systems. An essential element of this approach is the determination of absolute, fundamental quantities such as species concentrations, temperatures, and production and loss rates in subscale, midscale, and higher systems, which can be compared directly to predictions from fundamental and scaling models. Building a high-energy laser system based on preconceived, untested model predictions is not likely to lead to success. We have applied this diagnostic approach to a wide variety of complex systems including EOIL, catalytic-EOIL, micro-COIL, DPAL, and XPAL, and have shown several examples of those applications in this paper. Early versions of some of these diagnostics were critical in the development of high power COIL systems. For EOIL and related systems, we can comprehensively determine the operational parametrics, using quantitative measurements of $O_2(a)$ yield vs. small-signal gain, I_2 dissociation, and the effects of O and O_3. These balanced measurements of all of the major reacting species constrain the models, and enable the modifications necessary to upgrade their content.

Our work on the alkali laser systems is still in a developing stage, although we have used quantitative emission, absorption, and laser-induced fluorescence spectroscopy to investigate the fundamentals of the XPAL exciplex effect as discussed elsewhere.[11,12] We have focused here on new results from our laboratory in the development of quantitative gain and gain imaging measurements for DPAL configurations. We believe these techniques will be extremely important to diagnose the phenomenology and design optical resonators as DPAL systems are scaled to higher powers with side-pumping by high-energy diode lasers. We are also working to extend the method to XPAL applications.

In the development of these portable, compact diagnostic systems, we have chosen methods with extreme sensitivity and dynamic range so that they can be equally well applied to small scale and large scale systems. In particular, our EOIL-related investigations of discharge excitation kinetics, active oxygen chemistry, and I* production and loss mechanisms have benefited greatly from the high sensitivity for $O_2(a)$, O, I*, gain, and O_3; this sensitivity allows the use of low pressures and small reagent concentrations to limit the chemistry to a select few primary reactions, and leaves no doubt about the causes of the observed phenomena. We have found that the measurements at the subscale of a few Torr and a few mmole/s translate well to mid-scale conditions appropriate for "real" EOIL operation, i.e. the basic phenomenology behaves the same way in both cases. This consistency leads to the development of reliable models to guide the scaling of such systems to higher power and efficiency.

ACKNOWLEDGEMENTS

We are grateful for support from several U.S. government agencies who have funded portions of our diagnostics development activities and related research: Air Force Office of Scientific Research, High Energy Laser Joint Technology Office, Air Force Research Laboratory, and Defense Advanced Research Projects Agency. This work has benefited greatly from close collaborations with many colleagues: at CU Aerospace and University of Illinois Urbana Champaign: David Carroll, Wayne Solomon, Joe Verdeyen, Gary Eden, Joe Zimmerman, Andrew Palla, Brian Woodard, Gabriel Benavides; at Emory University, Michael Heaven; at MIT, Carol Livermore; at AFRL: Tim Madden and David Hostutler; and at PSI: Daniel Maser, David Oakes, and Lawrence Piper.

The views, opinions, and/or findings contained in this article/presentation are those of the author/presenter and should not be interpreted as representing the official views or policies, either expressed or implied, of the Defense Advanced Research Projects Agency or the Department of Defense.

REFERENCES

[1] Davis, S.J., Kessler, W.J., Keating, P.B., "Progress in the Development of Sensors for COIL Devices," Proc. SPIE Paper 3931-24, Gas, Chemical, and Electrical Lasers and Intense Beam Control and Applications," San Jose CA (2000).

[2] Davis, S.J., Rawlins, W.T., Kessler, W.J., Lee, S., Hunter, A.J.R., Silva, M.L. "Next Generation Diagnostics for COIL: New Approaches for Measuring Critical Parameters," (Invited Paper), Proc. SPIE Paper 5777-05, IV International Symposium on Gas Flow, Chemical Lasers, and High-Power Lasers, Prague, Czech Republic (2004)

[3] Rawlins, W.T., Lee, S., Kessler, W.J., and Davis, S.J., "Observations of Gain on the I($^2P_{1/2}\rightarrow{}^2P_{3/2}$) Transition by Energy Transfer from $O_2(a^1\Delta_g)$ Generated by a Microwave Discharge in a Subsonic Flow Reactor," Appl. Phys. Lett. 86, 051105 (2005).

[4] Rawlins, W.T., Lee, S., Kessler, W.J., Piper, L.G., and Davis, S.J., "Advanced Diagnostics and Kinetics of Oxygen-Iodine Laser Systems," AIAA-2005-5299, 36th AIAA Plasmadynamics and Lasers Conference, Toronto, Ontario, Canada (2005).

[5] Rawlins, W.T., Lee, S., and Davis, S.J., "Kinetics of Oxygen Discharges and I($^2P_{1/2}$) Excitation for EOIL," Proc. SPIE Paper 6454-18, LASE 2007 High-Energy/Average Power Lasers and Intense Beam Applications, San Jose CA (2007).

[6] Rawlins, W.T., Lee, S., and Davis, S.J., "Production of Metastable Singlet Oxygen in the Reaction of Nitric Oxide with Active Oxygen," Proc. SPIE Paper 6874-8, LASE 2008 High-Energy/Average Power Lasers and Intense Beam Applications, San Jose CA (2008).

[7] Rawlins, W.T. et al., "Efficient Electric Oxygen Iodine Laser," PSI-1513/TR-2344, Final Report for Contract FA9451-06-C-0196, AFRL/DELC, Kirtland AFB, NM, July 2008; Davis, S.J., Lee, S., Oakes, D.B., Haney, J., Magill, J.C., Paulsen, D.A., Cataldi, P., Galbally-Kinney, K.L., Vu, D., Polex, J., Kessler, W.J., and Rawlins, W.T., "EOIL Power Scaling in a 1-5 kW Supersonic Discharge-Flow Reactor," SPIE Vol. 6874, Paper 10 (2008).

[8] Rawlins, W.T., Lee, S., Hicks, A.J., Konen, I.M., Plumb, E.P., Oakes, D.B., and Davis, S.J., "Kinetics and Scaling of Gain and Lasing in a 1-5 kW Microwave Discharge Oxygen Iodine Laser," Proc. SPIE Paper 7581-03, LASE 2010 High Energy/Average Power Lasers and Intense Beam Applications, San Francisco CA (2010).

[9] Woodard, B.S., Zimmerman, J.W., Benavides, G.F., Carroll, D.L., Verdeyen, J.T., Palla, A.D., Field, T.H., Solomon, W.C., Lee, S., Rawlins, W.T., and Davis, S.J., "Demonstration of an Iodine Laser Pumped by an Air-Helium Electric Discharge," J. Appl. Phys. D 43, 025208 (2010).

[10] Hill, T.F., Velasquez-Garcia, L.F., Wilhite, B.A., Rawlins, W.T., Lee, S., Davis, S.J., Jensen, K.F., Epstein, A.H., and Livermore, C., "A MEMS Singlet Oxygen Generator - Part II: Experimental Exploration of the Performance Space," J. Microelectromechanical Systems 16, 1492-1505 (2007).

[11] Davis, S.J., Galbally-Kinney, K.L., Kessler, W.J., and Rawlins, W.T., "Spectroscopic Studies of Alkali Atom-Rare Gas Systems," Proc. SPIE 7581-21, LASE 2010 High Energy/Average Power Lasers and Intense Beam Applications, San Francisco CA (2010).

[12] Galbally-Kinney, K.L., Kessler, W.J., Rawlins, W.T., and Davis, S.J., "Dynamics of Optically Pumped Alkali Atom-Rare Gas Systems," AIAA-2010-5044, 41st AIAA Plasmadynamics and Lasers Conference, Chicago, IL (2010).

[13] Carroll, D.L., Verdeyen, J.T., King, D.M., Zimmerman, J.W., Laystrom, J.K., Woodard, B.S., Richardson, N., Kittell, K., Kushner, M.J., and Solomon, W.C., "Measurement of Positive Gain on the 1315 nm Transition of Atomic Iodine Pumped by $O_2(a^1\Delta)$ Produced in an Electric Discharge," Appl. Phys. Lett. 85, 1320-1322 (2004).

[14] Carroll, D.L., Verdeyen, J.T., King, D.M., Zimmerman, J.W., Laystrom, J.K., Woodard, B.S., Benavides, G.F., Kittell, K., Stafford, D.S., Kushner, M.J., and Solomon, W.C., "Continuous-Wave Laser Oscillation on the 1315 nm Transition of Atomic Iodine Pumped by $O_2(a^1\Delta)$ Produced in an Electric Discharge," Appl. Phys. Lett. 86, 111104 (2005).
[15] Carroll, D.L., Benavides, G.F., Zimmerman, J.W., Woodard, B.S., Palla, A.D., Verdeyen, J.T., and Solomon, W.C., "Enhanced performance of an electric oxygen-iodine laser," Proc. SPIE Vol. # 7581, Paper No. 7581-1, presented at LASE 2010, High Energy/Average Power Lasers and Intense Beam Applications V, SPIE Photonics West Conference, San Francisco, CA (2010).
[16] Lee, S., Rawlins, W.T., and Davis, S.J., "Surface-Catalyzed Singlet Oxygen Production on Iodine Oxide Films", Chem. Phys. Lett. 469, 68-70 (2009).
[17] Lee, S., Rawlins, W.T., and Davis, S.J., "Catalytically Enhanced Singlet Oxygen for EOIL," Proc. SPIE Paper 7196-04, LASE 2009 High Energy/Average Power Lasers and Intense Beam Applications, San Jose CA (2009).
[18] Rawlins, W.T., Lee, S., Hicks, A.J., Konen, I.M., Plumb, E.P., and Davis, S.J., "Catalytic Enhancement of Singlet Oxygen for Hybrid Electric Discharge Oxygen-Iodine Laser Systems," Proc. SPIE 7581-06, LASE 2010 High Energy/Average Power Lasers and Intense Beam Applications, San Francisco CA (2010).
[19] Rawlins, W.T., Lee, S., Hicks, A.J., Konen, I.M., Plumb, E.P., and Davis, S.J., "Catalytic Enhancement of Singlet Oxygen for Hybrid Electric Discharge Oxygen-Iodine Laser Systems," AIAA-2010-5043, 41st AIAA Plasmadynamics and Lasers Conference, Chicago, IL (2010).
[20] Herzberg, G., Molecular Spectra and Molecular Structure I. Spectra of Diatomic Molecules, Van Nostrand, New York (1951).
[21] Lafferty, W.J., Solodov, A.M., Lugez, C.L., and Fraser, G.T., "Rotational Line Strengths and Self-Pressure-Broadening Coefficients for the 1.27 μm, $a^1\Delta_g$ - $X^3\Sigma_g^-$, v = 0-0 Band of O_2," Appl. Opt. 37, 2264-2270 (1998).
[22] Newman, S.M., Lane, I.C., Orr-Ewing, A.J., Newnham, D.A., and Ballard, J., "Integrated Absorption Intensity and Einstein Coefficients for the O_2 $a^1\Delta_g$ – $X^3\Sigma_g^-$(0,0) Transition: A Comparison of Cavity Ringdown and High Resolution Fourier Transform Spectroscopy with a Long-Path Absorption Cell," J. Chem. Phys. 110, 10749-10757 (1999).
[23] Engleman, R., Jr., Palmer, B.A., and Davis, S.J., "Transition Probability and Collision Broadening of the 1.3 μm Transition of Atomic Iodine," J. Opt. Soc. Am. 73, 1585-1589 (1983).
[24] Krupenie, P.H., "The Spectrum of Molecular Oxygen," J. Phys. Chem. Ref. Data 1, 423-534 (1972).
[25] Piper, L.G. and Rawlins, W.T., unpublished work.
[26] Badger, R.M., Wright, A.C., and Whitlock, R.F., "Absolute Intensities of the Discrete and Continuous Absorption Bands of Oxygen Gas at 1.26 and 1.065 μm and the Radiative Lifetime of the $^1\Delta_g$ State of Oxygen," J. Chem. Phys. 43, 4345-4350 (1965).
[27] Slanger, T.G. and Copeland, R.A., "Energetic Oxygen in the Upper Atmosphere and the Laboratory," Chem. Rev. 103, 4095-4130 (2003).
[28] Rawlins, W.T., Caledonia, G.E., and Armstrong, R.A., "Dynamics of Vibrationally Excited Ozone Formed by Three-Body Recombination. II. Kinetics and Mechanism," J. Chem. Phys. 87, 5209-5221 (1987).
[29] Palla, A.D., Verdeyen, J.T., and Carroll, D.L., "Exciplex Pumped Alkali Laser (XPAL) Modeling and Theory," XVIII International Symposium on Gas Flow and Chemical Lasers and High Power Lasers 2010, Paper AO 10 (2010).